Manufacturing Of Carbon-Supported Platinum Cathodes For Proton Exchange Membrane Fuel Cell Using The Doctor Blade Process: Microstructure And Performance

Clémence Lafforgue, Pierre Toudret, Fabrice Micoud, Marie Heitzmann, Jean-François Blachot, Marian Chatenet

Manufacturing Of Carbon-Supported Platinum Cathodes For Proton Exchange Membrane Fuel Cell Using The Doctor Blade Process: Microstructure And Performance

Clémence Lafforgue[1-2], Pierre Toudret[1], Fabrice Micoud[1], Marie Heitzmann[1], Jean-François Blachot[1] and Marian Chatenet[2,&]

[1] *Univ. Grenoble Alpes, CEA, LITEN, DEHT, 38000 Grenoble, France*

[2] *Univ. Grenoble Alpes, Univ. Savoie Mont Blanc, CNRS, Grenoble INP*, LEPMI, 38000 Grenoble, France*

*Institute of Engineering and Management Univ. Grenoble Alpes

[&] Marian.Chatenet@grenoble-inp.fr

Abstract

Catalyst layers (CL, the anode and cathode) properties do influence the performance of proton exchange membrane fuel cells (PEMFC). CLs are prepared by depositing an ink made from a catalyst (carbon-supported Pt-based nanoparticles, NPs) and an ionomer in appropriate solvents on a substrate, followed by post-treatment (solvent evaporation, calendaring, hot-pressing). The literature rarely provides details and characterizations about CLs fabrication. This contribution investigates a way to prepare Pt/VC (Pt NPs supported on Vulcan XC72 carbon-black) and Pt/GC (Pt NPs supported on graphitized-carbon-black) PEMFC CLs. The ink formulation, mixing and deposition methods are evaluated and the areal homogeneity/texture of the formed CLs thoroughly characterized by scanning electron microscopy and X-Ray fluorescence. Light-ball-milling mixing enables to prepare homogeneous and agglomerate-free inks without degrading the Pt/C catalysts. The optimal ionomer-to-carbon ratio differs for Pt/GC and Pt/VC CLs; it not only depends on the BET surface area of the carbon substrate and its outer apparent surface (apparent carbon particles diameter), but should also be adapted to physicochemical surface properties of the Pt/C sample. Optimized I/C = 1-1.2 enables to improve the performance of Pt/GC cathodes by *ca*. 300% *versus* I/C = 0.5 (at 80°C, 80%RH), owing to hugely-depreciated proton-transport-resistance in the CL.

Keyword: Proton exchange membrane fuel cell (PEMFC), catalyst ink, membrane-electrode

assembly (MEA), catalyst layer, ionomer to carbon ratio, X-ray fluorescence spectroscopy

1 Introduction

Global warming and related climate change calls for a redefinition of our energy policies [1]. Producing more renewable electricity should enable to reduce our consumption of fossil fuels, but this requires efficient means to store it [2], as renewable sources are by nature intermittent. Power-to-gas and in particular power-to-hydrogen (molecular hydrogen, H_2) is amongst the targeted technologies to store renewable electricity [3]. Then, H_2 can be either used in the industry as a raw chemical or oxidized in fuel cells to generate electrical power. In the transportation sector, low-temperature fuel cells and more specifically proton exchange membrane fuel cells (PEMFCs) systems have assets, such as fast fuel refilling and high energy density compared to battery-powered vehicles [4]. PEMFCs are however still limited by their high cost, due to the use of expensive core materials, such as platinum-based catalysts, and by their still too-limited durability in operation [5, 6]. The areal loading of platinum needs to be minimized in practical cells, without compromising neither their performance nor their durability; this is not an easy task [7]. The intrinsic activity of catalysts must be enhanced and they must also be properly integrated by an appropriate combination with the proton-conducting ionomer into the so-called catalyst layers (CLs) [8]. A proper interface between the catalyst material (typically, carbon-supported platinum nanoparticles: Pt/C or PtM/C, with M being an alloying element, Ru, Co, Ni, etc.) and the ionomer is pivotal to obtain high-performance CLs, notably at the cathode, the limiting electrode in a PEMFC [9-11]. While there is an abundant literature that describes the links between the CL structure and the performance [12-14], the knowledge to obtain a “good” CL is still insufficient. To be more specific, this knowledge mostly results from trial-and-error methodologies, most of which being proprietary (i.e. not shared in the research community). Papers addressing the methodologies to prepare “good” CLs and membrane electrode assemblies (MEAs) are scarce, e.g. [15-17], and many of them are specific to particularly functionalized carbon supports (and sometimes highly-oxygen permeable (unconventional) ionomers) [18, 19], and their conclusions may not be generalized to widely-used commercial carbon-supported electrocatalysts.

The keys to “good” properties of the catalyst layers are multifold. Firstly, the various components of the CL (catalyst and ionomer) should be mixed appropriately, creating homogeneous inks [20]. The nature of the ink components (type of catalyst and notably of the carbon support, type of ionomer, nature of the solvents) and their relative proportions have a significant impact on the ink homogeneity and the catalyst layer properties [21-24]. The order of introduction of components to create the ink and the method of mixing are crucial to obtain

an homogeneous ink without agglomerates of catalysts and/or ionomer, that could result in depreciated PEMFC performance and durability [25]. Secondly, once this ink has been obtained, the process to form the CL should be chosen appropriately. The ink properties and notably its viscosity should be adapted to the deposition process. Bar coating using a doctor blade, ultrasonic spray deposition or screen-printing are usual techniques encountered in the literature (see e.g. [15, 26]). After deposition and drying, the catalyst layers must be assembled with the membrane and gas diffusion layers (GDL) to form the membrane-electrode assembly (MEA). One of the most common processes used for this is the decal transfer process. It consists of depositing the catalytic ink on an inert substrate and, after drying, transferring the catalyst layers from the substrate to the membrane using a hot pressing step. The transfer parameters such as temperature, pressure and time of the hot pressing step should be adapted for each catalyst layer [27, 28]. The assembly of catalyst layers and membrane is called catalyst-coated membrane (CCM). The GDLs are then added to form the MEA. Therefore, the production of the catalyst layers and their assembly to form an MEA involves a very large number of parameters that need to be adjusted.

At present, there is no universal recipe to create a “good” CL. Some information is however present in the literature [10, 11]. For example, for Pt nanoparticles (NPs) supported on carbons presenting high surface area and Nafion®-type ionomers, the usual ionomer content of the dry CL is on the order of 30 wt%. High ionomer content is favorable to proton conduction but prevents O_2 transport, while the situation is reversed at low ionomer content [12, 29]. Usual solvent of the catalytic ink, is water alcohol mixture containing light alcohols easily evaporated and not critical to the environment like ethanol, n-propanol or 2-propanol (IPA) [30-32]. The nature of the alcohol as well as the water / alcohol ratio have an important impact on the ink properties, hence on the CL structure and the PEMFC performance and durability [31, 33, 34]. The ink mixing is conventionally performed using ultrasonic bath and/or probe, or batch dispersers (e.g. ultra-turrax®), or ball-milling, or a combination of these. However, in many papers, the information regarding the complete procedure of MEA preparation does not enable to be fully reproduced.

To start filling this gap, the present paper aims to provide a detailed and practical methodology to prepare MEAs using low-loaded (0.1 mg cm^{-2} Pt areal loading) Pt/graphitic carbon (Pt/GC) electrode and Pt/Vulcan XC72 electrode, with a conventional PerFluoroSulfonic Acid (PFSA) ionomer and membrane. In this study, the graphitic carbon-based catalyst (and related electrode) is used at the cathode and the Vulcan-based catalyst at the anode. The chosen methodology to coat the catalyst layer is the blade coating on a PTFE sheet, followed by decal transfer onto the membrane. Upon preparation, these CLs are fully characterized by physicochemical means, in terms of thickness, homogeneity, presence of defects and agglomerates and areal Pt loading. CLs are also electrochemically characterized by

electrochemical surface area (ECSA) measurement, polarization curves and electrochemical impedance spectroscopy (EIS).

2 Experimental section

2.1 Materials

Two commercial catalysts were used in this study, coming from Tanaka Kikinzoku Kogyo (TKK). The cathode catalyst consists of 30 wt% Pt nanoparticles supported on graphitized carbon black (reference TEC10EA30E-HT from TKK, named “Pt/GC” in this study). The anode catalyst consists of 47 wt% Pt nanoparticles supported on Vulcan XC72 carbon black (reference TEC10V50E from TKK, named “Pt/VC” in this study) [35, 36]. The ionomer dispersion is a 20 wt% Nafion® dispersion in a mixture of 34 wt% water and 46 wt% 1-propanol (D2020, Chemours). The ink solvent consisted of a mixture between ethanol and ultrapure water (Direct Q-3UV, Merck, resistivity = 18.2 MΩ cm, < 5 ppb total organic carbon, TOC). For all MEA, a 15 µm thick PerFluoroSulfonic Acid (PFSA) membrane was used (MX820.15, Gore®) with a 215 µm thick gas diffusion layer (GDL) with a microporous layer (MPL) (22BB, SGL carbon).

2.2 Catalyst ink preparation

Two main methods of ink preparation were tested herein for the anode and cathode inks, and the general flowcharts of the processes are described in **Figure SI-1**.

The first one is to mix all the components in a 60 mL plastic flask in the following order: catalyst powder, ultrapure water, ethanol and ionomer dispersion (water is necessarily added before the alcohol to avoid ignition of Pt in contact with ethanol vapor). Then the ink is mixed with a magnetic bar overnight at 400 rpm.

The second one is to first mix, in the following order, the catalyst powder with ultrapure water and ethanol. The components were added in a 60 mL plastic flask with 30 g of 3 mm diameter ZrO_2 beads and the ink is mixed overnight with a roller mill (roller 10 basic, IKA) at 30 rpm at room temperature. This technique was inspired by the works of Gasteiger and is called herein “light-ball-milling” (LBM) [31, 37, 38]. The next day, the ionomer dispersion is added to the vial and the solution is mixed again with the roller mill at 30 rpm all night and for 2 days for the anode ink and the cathode ink, respectively. **Figure 1A** illustrates the way the ink is homogenized in method 2.

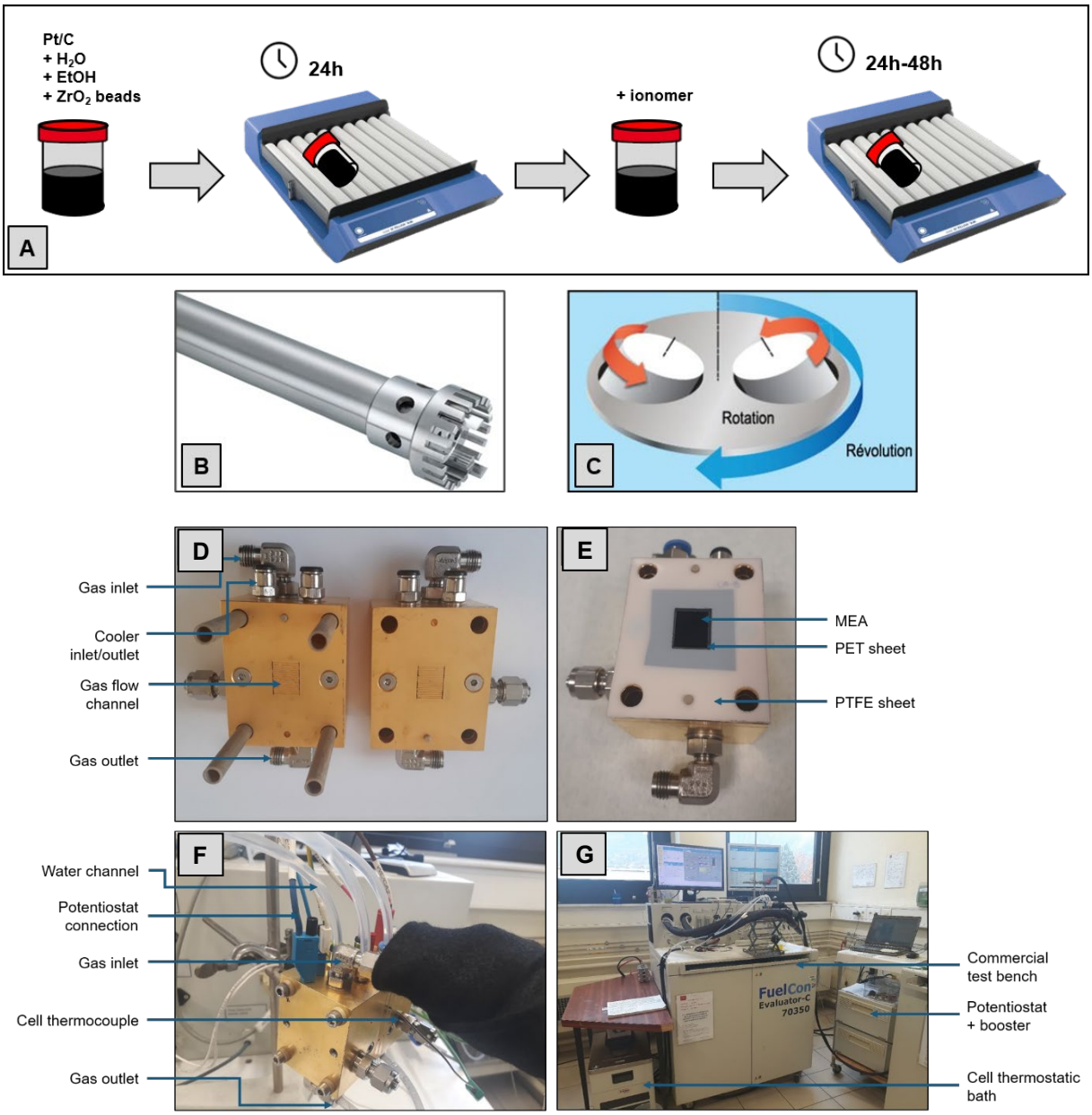

Figure 1. Illustration of the ink preparation and homogenization protocol using (A) the roller mill (method 2), (B) the Ultra-Turrax or (C) the Kurabo. (D), (E) Pictures of the electrochemical cell's core, (F) Pictures of the electrochemical cell set up on the commercial test bench and (G) Pictures of the test bench with the potentiostat and the cell thermostatic bath.

For both methods, the whole ink is used right after the final dispersion step. For the cathode inks using 30wt% Pt nanoparticles on graphitized carbon black, Pt/GC, four ionomer/carbon mass ratio were tested: I/C = 0.5, 0.7, 1 and 1.2. The water/ethanol volume ratio was 4.2. For the anode ink using 47wt% Pt nanoparticles on Vulcan XC72 carbon black, Pt/VC, the ionomer/carbon mass ratio was fixed at 0.7 and the water/ethanol volume ratio was 3.8. It has been decided to add the ionomer after a first step of dispersion in order to break the catalyst agglomerate so to optimize the distribution of the ionomer around the particles in the best possible manner, as previously studied in [39].

To go beyond, the first method was modified both for the Pt/VC anode and the Pt/GC cathode inks, replacing the magnetic stirring by other traditional means of mixing: (i) mixing in ultrasonic bath (Fischer scientific, FB 15048, 50 Hz, 20 min), (ii) mixing with an ultrasonic probe (Ultrasonic Processor Qsonica® P700 with 1/2" diameter probe 20 kHz, 1 min, amplitude 10%, 4s ON / 4s OFF), (iii) mixing with an ultra-Turrax (IKA ULTRA-TURRAX® T 18 digital, 5 min 8000 rpm) (**Figure 1B**) or (iv) mixing with a planetary mixer deaerator (Kurabo Mazerustar KEOL M400WE-G2, program 4 (first step : 30 s / revolution = 3 / rotation = 9, second step : 120 s / revolution = 9 / rotation = 5, third step : 120 s / revolution = 9 / rotation = 1) (**Figure 1C**).

2.3 MEA preparation

Using the inks being prepared as detailed above, CCM were prepared using doctor blade process using an automatic film coater (Elcometer). The CLs were deposited on a PTFE sheet, and then transferred onto the proton exchange membrane by hot pressing, using a set of parameters (temperature, pressure and hot-pressing time) enabling any catalyst layer to be transferred, whatever its composition. More specifically, inks were coated on a 250 µm thick PTFE sheet (10 cm x 13 cm) that was immobilized flat on a vacuum and heating plate set at 60°C. The coating speed was set to 5 $mm.s^{-1}$ and the coating was dried on the heating plate for approximately 5 min. The platinum targeted loading was 0.1 $mg.cm^{-2}$ for both the anode and cathode CLs. Then the CLs were transferred onto the membrane using a metal mold and a press equipped with hot plates (Syntax 100, 3R). The mold was first pressed at 50 N for 3 min at 140°C to obtain a homogeneous heat distribution. Then the mold was pressed at 1 MPa for 5 min at 140°C. The final MEA was a square of 25 cm^2 that was cut into 4 samples for the performance measurements in differential cell (**Figure 1D-G,** see below for details).

2.4 Estimation of Pt loading in the catalyst layers

The most straightforward and widely used method to estimate the final areal loading of Pt in the catalyst layers is to weigh the substrate before and after the coating. Knowing the weight percentage of Pt in the dry extract, it is possible to calculate the average of the Pt loading. However, this technique does not allow to determine if the Pt loading is homogeneous on the whole surface of the coating, and is suffering high uncertainty if low loadings are targeted. Thus, inspired by the work of Mauger *et al*. which used *in situ* X-ray Scattering [25], another technique has been tested here, the X-ray fluorescence spectroscopy, XRF (XDV-SDD, Fisherscope). This technique is very interesting because it is non-destructive, is quite fast to use and is suitable for very low-loaded coatings (< 0.1 mg_{Pt} cm^{-2}). The catalytic layers being 7 cm wide and 10 cm long, the coatings were analyzed over 70 points (excluding the edges of 1 cm), each point being exposed to X-ray for 30 seconds with a 3 mm diameter collimator. The results can be plotted on a surface-type graph, which allows to visualize easily the distribution of Pt on the whole surface of the sample, hence the homogeneity of the CL deposits onto the PTFE substrate.

2.5 Microstructure analysis of the coatings

Field-Emission Gun Scanning Electron Microscopy (FEG-SEM) characterizations were done on both the coated electrodes (surface analysis) and the final MEA (cross section analysis) in order to evaluate the presence of agglomerates or cracks and to observe the interface between the membrane and the catalyst layer. Four samples were spatially and randomly cut in the electrodes and one sample was cut from the final 25 cm^2 MEA. The analyses were conducted with a FEG-SEM LEO 1530 from Zeiss and several images and measurements were performed on each sample.

Transmission electron microscopy (TEM) experiments were performed on the two pristine catalyst powders, using a Jeol 2010 microscope equipped with a LaB6 filament, as detailed in [40].

2.6 Electrochemical cell and test bench

The electrochemical measurements were performed using a differential cell of PEMFC equipped with straight and parallel gas flow channels (250 µm/250 µm rib/channel widths and 400 µm depth) at both anode and cathode sides. This small electrochemical cell with an active area of 1.8 cm² was designed to guarantee a homogeneous operation in the plane between the gas inlet and the gas outlet using high stoichiometry of gases (50 at 1 A cm^{-2} for both hydrogen and oxygen/air) and so to investigate the MEA performance under ideal and well-controlled conditions. 150 µm thick PTFE sheets, with a rectangular opening of 14 mm x 17 mm where the GDL were positioned, guarantee airtightness and proper GDL compression (around 20%, in line with the providers instructions). 25 µm thick polyethylene terephthalate (PET) sheets with a rectangular opening of 12 mm x 15 mm allow to maintain the MEA and to define the 1.8 cm² active area. These various components are placed in the cell as follows: 1) PTFE sheet + GDL in the center, 2) PET sheet, 3) CCM, 4) PET sheet, 5) PTFE sheet + GDL in the center.

The electrochemical cell was tested using on a commercial test bench (Evaluator C 70350, FuelCon) that supplies each of the humidified gases (H_2, N_2, O_2 and air) to the cell at the desired flow rate and pressure (**Table 1**). The gas dispensing lines are heated in order to prevent water condensation (at $T = T_{cell} + 30°C$). Deionized water is used as cooling liquid to maintain the cell at the chosen operating temperature. The temperature of the cell and gas dispensing lines are controlled thanks to several thermocouples.

For all the electrochemical measurements, the cell was connected to a potentiostat and a booster (VMP3, Biologic®) to control and register the cell potential and current (using the EC-Lab® software). The anode is considered as the counter and reference electrodes in these conditions, the cell being cathode-limited.

Figure 1D-G shows the differential cell fixture, MEA and fuel cell test bench.

2.7 Electrochemical measurements

Prior to any electrochemical measurements, a break-in protocol was performed under H_2 / (O_2 + N_2) in order to humidify the membrane and reach the maximum performance of the MEA. To do so, the cell potential was maintained for 30 min at E = 0.2 V, T = 80°C, 80% RH and P = 1.5 bar abs as in-house protocol for these low-loaded MEA. The tested operating conditions are recalled in **Table 1**.

Polarization curves were performed under H_2 / (O_2 + N_2, 21% O_2) from U = open circuit voltage (OCV) to U = 0.1 V at v = 10 mV s^{-1}, T = 80°C, P = 2 bar abs. It will be considered hereafter that these cell voltages are in first order equivalent to the cathode potential values. Two cycles of voltammetry were performed in each case and three relative humidity values were tested: 50, 80 and 100% RH.

Electrochemical impedance spectra (EIS) were acquired in order to gain insights into the resistive phenomena ruling the cell performance, notably the high frequency resistance of the MEA. Prior to EIS acquisition, the cell voltage was maintained at the desired voltage/cathode potential for 2 min (the EIS measurements have been made at U = 0.85, 0.65, 0.5 and 0.3 V). Then EIS was acquired from 100 kHz to 1 Hz, with a ± 10 mV amplitude, at E = 0.85, 0.65, 0.5 and 0.3 V. The mean of the high-frequency resistances measured at these four different voltages have been used to correct the polarization curves of the ohmic-drop; all the polarization curves presented hereafter correspond to R_{HF}-free cell voltage.

Finally, three cycles of cycling voltammetry (CV) were performed under H_2 / N_2 from U = 0.1 V to 1.2 V at v = 50, 100 and 200 mV s^{-1}. The results presented in the rest of the study were obtained for a sweep speed of 100 mV.s^{-1}. Then EIS diagrams were acquired at U = 0.4 V from f = 100 kHz to f = 1 Hz with a ± 10 mV amplitude to evaluate the proton transport resistance of the cathode CL (see the “Proton resistance measurements” section in supporting information for further details).

Table 1. Operating conditions used for the electrochemical test protocols. The pressures are expressed in bar abs.

Comments	T_{cell} (°C)	P (bar)	RH (%)	Q_{H2} (NLh)	Q_{N2} (NLh)	Q_{O2} (NLh)	P_{H2O} (bar)	P_{N2} (bar)	P_{O2} (bar)
Break-in	80	1.5	80	38	75	20	0.4	0.9	0.2
Pol. curve	80	2	50	38	34	10	0.2	1.4	0.4
	80	2	80	38	30	10	0.4	1.2	0.4
	80	2	100	38	28	10	0.5	1.1	0.4
ECSA	30	0	100	38	95	0			

3 Results and discussion

3.1 Catalyst layers and MEA characterization

In this work, it was chosen to start with commercial components to prepare the MEAs. As far as the cathode and anode catalysts were concerned, the materials were chosen among materials that have already been intensively evaluated in the past [41, 42]. These materials have therefore not been intensively characterized here on their own to start with, because their properties can be considered as common knowledge for people in the field (their oxygen reduction reaction, ORR, properties and ECSA are for example accessible in Ref. [40]). Nonetheless, **Figure 2** shows representative TEM micrographs at low and high magnification of the 30 wt% Pt nanoparticles supported on graphitized carbon black (Pt/GC) used at the cathode and the 47 wt% Pt nanoparticles supported on Vulcan XC72 carbon black (Pt/VC) used at the anode, both materials having been thoroughly characterized in an earlier contribution of some of the authors [40]. As expected, the micrographs illustrate that (i) the GC carbon is more graphitized than the VC one, (ii) the Pt nanoparticles are *ca* twice larger when supported on GC (6.3 nm) than on VC (2.8 nm) and (iii) the extent of agglomeration is larger for the Pt/VC material than for the Pt/GC one. This is in full agreement with earlier reports that deal with similar materials, e.g. [35, 36, 40].

Another clear observation from these TEM micrographs is that, despite very different BET area (ca. 240 and 120 $m^2.g^{-1}$ for the VC and GC, respectively, as specified from the provider of the catalysts), the individual particles of carbon have a similar outer diameter (around 30-50 nm). In other words, the larger BET area of VC mostly originates from its inner porosity, a feature that the more organized (graphitized) GC does not exhibit. This will have implication for the ink formulation and the MEA performances, as it will be discussed hereafter.

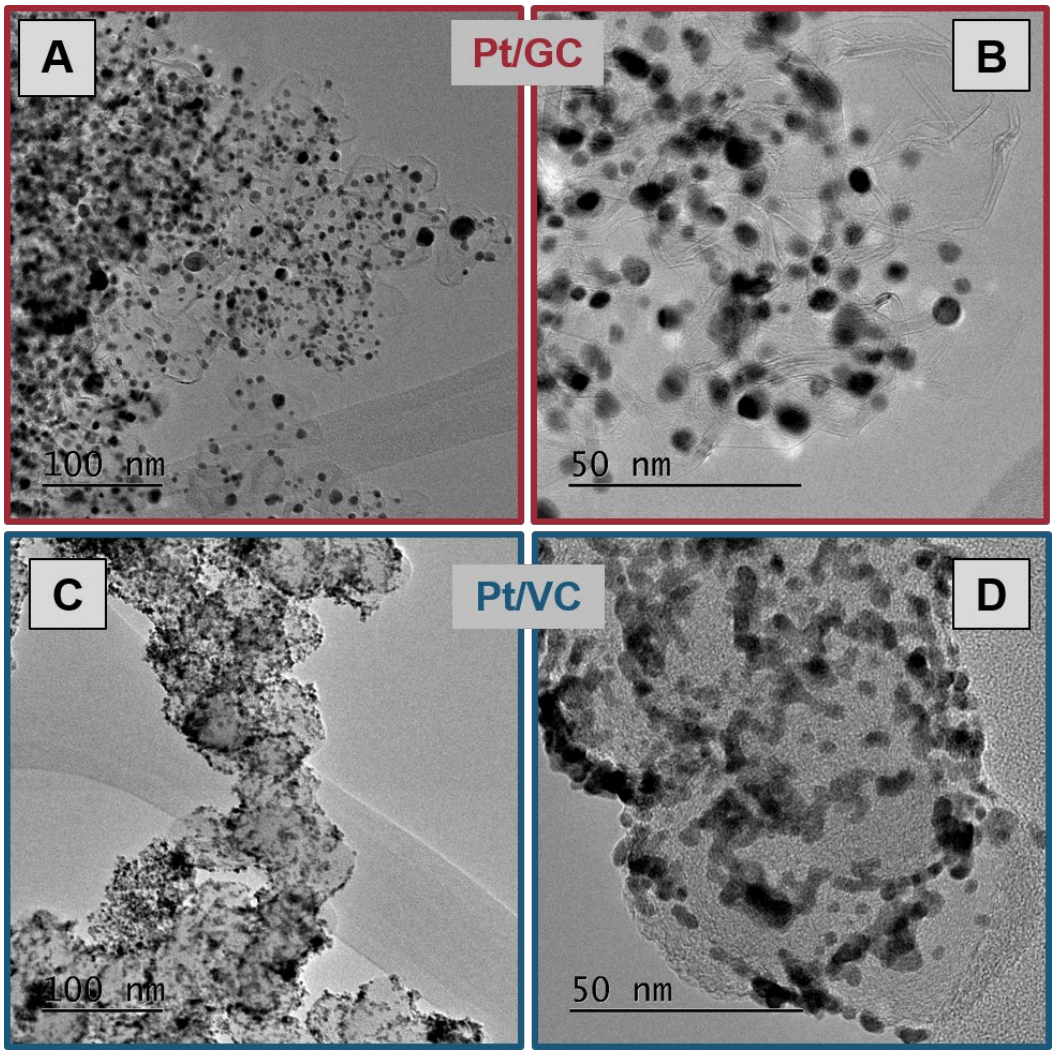

Figure 2. TEM images of the catalysts studied in this work: (A), (B) Pt/GC catalyst and (C), (D) Pt/VC catalyst.

Using these catalysts, inks were prepared as detailed in section 2.2 and then MEAs as detailed in section 2.3. The surface characterizations by SEM of **Figure 3** clearly show the very different state of surface obtained for CLs made by doctor blade coating, depending on the way the inks were mixed. This illustrates that not only the ink composition is important, as already stressed in numbers of reports for Nafion®-type ionomers [31, 33, 43, 44] or HOPI ones [19], but also the way the inks had been mixed [25, 43]. The order of addition of the components to the ink plays also a major role. In this study, it was decided to mix the catalyst powder and the solvents for 24 h prior ionomer addition, and another 24-48 h after ionomer addition, as detailed in [40, 45]. Adding the ionomer directly is problematic for two reasons: (i) the alcohol solvents (and vapors) of the ionomer solution may ignite by the Pt nanoparticles and (ii) although debated in the literature, this could result in ionomer pocket around Pt/C agglomerates in the initial ink, that are very difficult to break afterwards, at least without degrading the Pt/C catalysts [46]. Also, for the inks studied herein, magnetic stirring, which is a widely employed technique, is clearly not enough as it yields very defective CLs, with large agglomerates and cracks (**Figure 3A** for Pt/GC and **Figure 3C** for Pt/VC). On the contrary, light-ball-milling enables to obtain nearly defect-free CLs for these two catalysts (**Figure 3B, D**). Apart the light-ball-milling method, none of the other mixing techniques was effective in preventing the creation of such defective CLs, as further illustrated in **Figure SI-2** in supporting information. Moreover, the example of **Figure SI-3** demonstrates that the agglomerates are not linked to the blade coating protocol, but are present already in the inks (if it was not the case, the mixing process would not change the morphology of the obtained coatings).

From these results, one can conclude that the ink mixing procedure is pivotal to its properties; light-ball-milling seems to be the only method of mixing (among those considered in this work) that is efficient to break the agglomerates in the ink and to avoid major CL defects, at least with the present ink compositions (nature of solvents and of the catalyst: Pt/VC and Pt/GC) and active layer deposition technique (doctor blade on a PTFE decal).

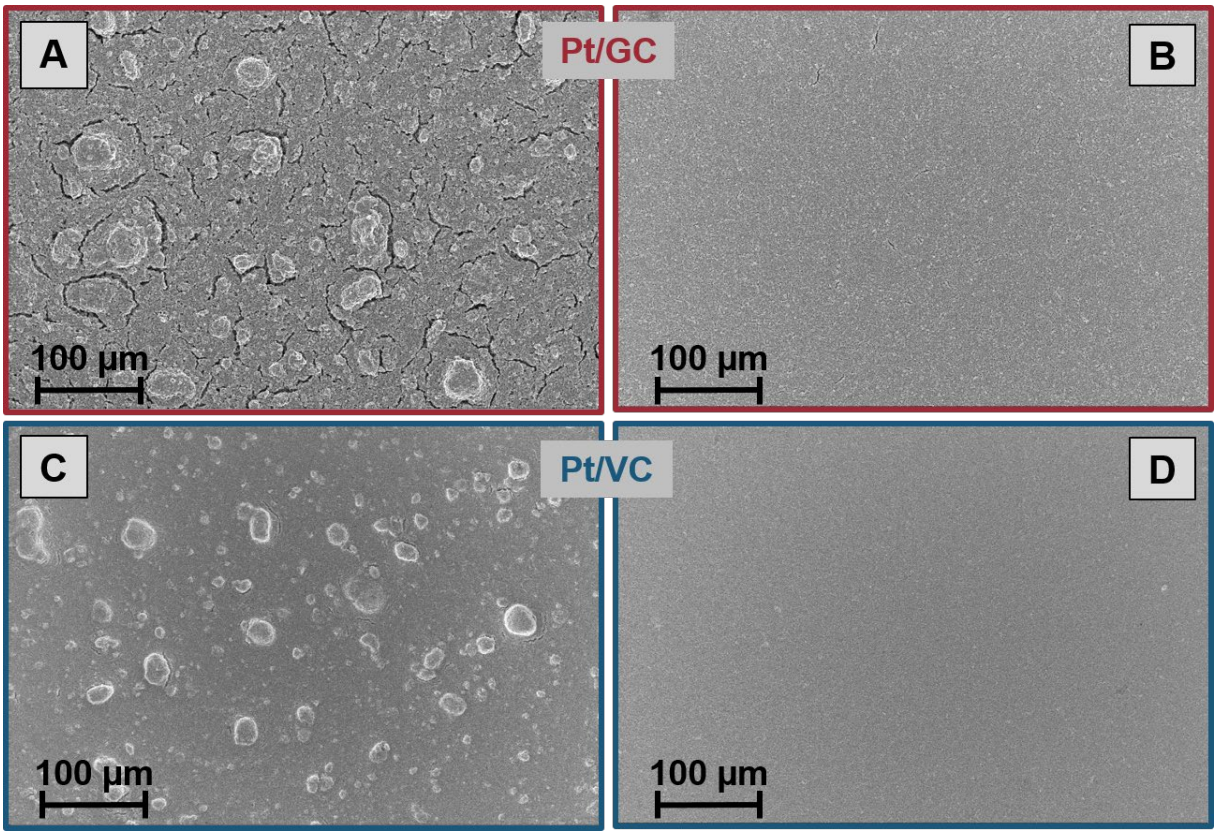

Figure 3. SEM micrographs of the doctor blade coatings obtained with (A) Pt/GC ink with magnetic mixing, (B) Pt/GC with light-ball-milling, (C) Pt/VC ink with magnetic mixing, (D) Pt/VC with light-ball-milling. The micrographs were always realized on the CL supported on the PTFE decal, *i.e.* prior transfer by hot-pressing onto the membrane.

The CL deposits obtained by mixing the ink with light-ball-milling were then characterized to evaluate the homogeneity of the coating from a CL thickness and Pt areal loading viewpoints. **Figure 4A** recalls the methodology of the XRF mapping performed to evaluate the local Pt areal loading of the prepared CLs, while **Figure 4B,C** give examples of the obtained data for Pt/GC and Pt/VC CLs prepared using inks mixed with light-ball-milling. Several conclusions can be derived from these images. Firstly, the targeted Pt areal loading of 0.1 mg_{Pt} cm^{-2} was obtained for the two catalysts, with an average loading of 0.09 ± 0.005 mg_{Pt} cm^{-2} for Pt/GC and 0.131 ± 0.012 mg_{Pt} cm^{-2} for Pt/VC CLs. Secondly and very importantly, if there are local variations from the average Pt areal loading, they are within ±15%, which can be considered low. These local variations are more pronounced in CLs obtained using magnetic stirring (**Figure SI-4**) and less marked with the light-ball-milling process (**Figure 4B,C**). One notes that the XRF maps are not markedly different for the CLs prepared by magnetic mixing or light-ball-milling, though, illustrating that the presence of agglomerates and defects do not necessary yield significant local variations of the Pt content at the CL surfaces, at least at the spatial definition accessible by the XRF measurements.

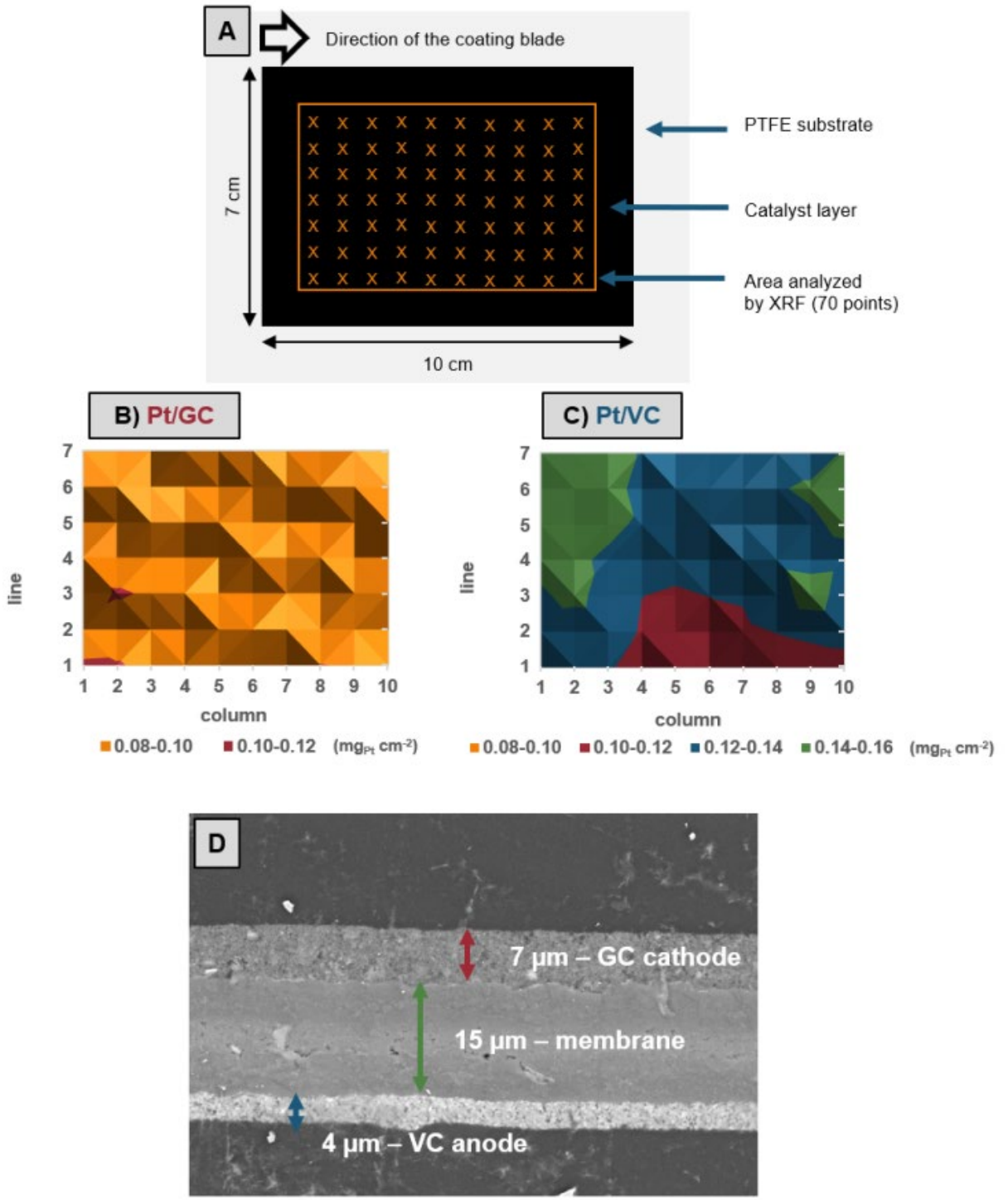

Figure 4. XRF characterizations: (A) Illustration of the real analyzed area of the coating; (B) Example of the XRF mapping of a Pt/GC coating and (C) Example of the XRF mapping of a Pt/VC coating, the CLs having been prepared with inks mixed by light-ball-milling. The XRF maps were realized on the CL supported on the PTFE decal, *i.e.* prior transfer by hot-pressing onto the membrane. (D) Corresponding cross-section SEM images of the Pt/GC coating (hereafter used at the cathode) and Pt/VC coating (hereafter used at the anode) for the MEA obtained by decal of the corresponding CLs on the membrane.

The corresponding SEM cross-section micrograph of the MEA prepared with inks mixed by light-ball-milling using Pt/VC electrode as anode and Pt/GC electrode as cathode (**Figure 4D**) confirms the homogeneous thickness of the deposits, when the ink is free of agglomerates. On the contrary, **Figure SI-5**, relative to similar measurements performed on MEAs assembled from CLs elaborated with improperly mixed inks (in that case by ultrasonic mixing and ultra-Turrax mixing), shows that the presence of agglomerates in the inks, hence in the CLs, leads to a significant deformation of the membrane once the CLs have been transferred by hot-pressing. Harsh local deformations of the membrane could result in abnormal operation and reduced durability of the MEAs.

In summary, among the different dispersion methods used in the study, only light-ball-milling allowed to obtain smooth CLs without any agglomerates or cracks (detected in SEM images) or heterogenous Pt areal loading (detected in XRF).

3.2 Electrochemical performance of the MEA

Figure 5A shows representative cyclic voltammograms (CVs) obtained for MEAs operated under H_2 / N_2 in high-humidity conditions (T_{cell} = 30°C, 100% RH) for a Pt/GC cathode at various ionomer/carbon mass ratios (I/C) and a Pt/VC anode. In these conditions, the Pt/VC anode (negative electrode in these conditions) plays the role of reference and counter-electrode, enabling to measure the voltammogram of the Pt/GC cathode (positive electrode in these conditions). There are no major differences of CV shape when the I/C ratio changes in the range 0.5 < I/C < 1.2. From this set of graphs, and in particular from reproducibility experiments, the active area of Pt (S_{Pt}, in cm^2_{Pt} cm^{-2}_{geom}) is determined for each CL from integration of the hydrogen underpotential deposition peaks (H_{UPD} method, see e.g. [40] for details). Then, the electrochemical surface area (ECSA, in m^2 g^{-1}_{Pt}) is calculated using the areal Pt loading of each Pt/GC cathode catalyst layer and the S_{Pt} values (**Table 2**); the ECSA corresponds to the total platinum surface area accessible to protons in the characterized CL (the so-called Pt utilization factor). Whatever the ionomer/carbon ratio, Pt/GC cathodes exhibit close values of S_{Pt} and ECSA. Nevertheless, an optimal I/C ratio, from the S_{Pt} and ECSA point of view, is found for I/C = 0.7; S_{Pt} and ECSA values remain inferior and near-similar for I/C = 0.5, 1 and 1.2. ECSA measurements performed at 80°C and 50%RH, or 80%RH, or 100%RH showed the same trends between ECSA and I/C (see **Figure SI-6**). However, the ECSAs measured at low relative humidity values (50%RH and 80%RH) were lower (about 15-25% lower) than those obtained at 100%RH, the difference noted between the various %RH being essentially insignificant at the various I/C values tested, within the error bar of the measurements. The smaller ECSA measured by proton desorption coulometry measured at

low %RH is due to the fact that the graphitized carbon support of the Pt/GC catalyst absorbs little water (there is no internal micro/meso porosity as that encountered in Pt/HSAC, for instance). This denotes for a smaller Pt utilization factor at low RH%. In the case of a more hydrophilic and porous carbon, such as an HSAC, the difference observed in the ECSA measurements as a function of relative humidity is smaller [47] (in other words, the Pt utilization varies less for a hydrophilic carbon substrate than for an hydrophobic one). In result, the GC support is not capable to "self-regulate" sufficient water content and is very sensitive to the relative humidity conditions and to the I/C ratio. Hence, (from the ECSA view point), an optimum of I/C ratio exists: at low (insufficient) ionomer content, not all Pt/GC sites are accessible to protons, because the ionomer phase is too "far" and protons have no access to the Pt sites, whereas at (too) high ionomer content, some Pt/GC particles/agglomerates become encapsulated in the ionomer (ionomer pockets), altering the electronic conduction to the Pt/GC sites. This is rather classical for non-hydrophilic (non-microporous) carbon supports and had been put forth by Litster *et al*. [12] two decades ago, and more recently by Gatto et al. [48] (for Aquivion®-based catalyst layers), Suzuki et al. [49] (for Nafion®-based catalyst layers) and Lee et al. [50].

Table 2 shows that the values of electrochemical surface area (ECSA, in $m^2\ g^{-1}_{Pt}$) measured at T_{cell} = 30°C, 100% RH are within ($24.4 < ECSA < 32.2\ m^2\ g^{-1}_{Pt}$) depending on the I/C ratio. These values match those found in the literature for this particular Pt/GC catalyst for an ink with I/C = 0.5, when measured in gas diffusion electrode (GDE: 13 and 28 $m^2\ g^{-1}_{Pt}$ when measured by H_{upd} and CO-stripping voltammetry, respectively) or differential cell (DC: 22 $m^2\ g^{-1}_{Pt}$ measured by H_{upd}) setups [40]. They are also significantly above the values measured in the same study in the rotating disk electrode (RDE) configuration (14 and 15 $m^2\ g^{-1}_{Pt}$ when measured by H_{upd} and CO-stripping voltammetry, respectively). The ECSA values in that latter case are likely lowered because of insufficient wetting of the hydrophobic Pt/GC thin-film catalyst layer by the liquid acid electrolyte in RDE [40], here again showing that hydrophobic carbon substrates may lead to large variations of the Pt utilization depending on the operating conditions. In any case, the ECSA values measured herein and in [40] for similar Pt/GC cathode CLs with I/C = 0.5 are very close (24.4 *vs*. 22 $m^2\ g^{-1}_{Pt}$ when measured by H_{upd}), which demonstrates that the present methodologies to prepare MEAs and to characterize them is robust. It must be noted, though, that the I/C ratio does not have a major influence on the measured active area of platinum (and ECSA) in the experimental conditions tested here, as values at I/C = 0.7, 1 or 1.2 only increase by 32, 14 and 5%, respectively, versus the value monitored at I/C = 0.5. The optimal value monitored at the intermediate I/C ratio of 0.7 translate the findings of Passalacqua et al. [13]: at low ionomer content, only some of the catalyst particles are ionically connected to the membrane; too much ionomer can electrically disconnect catalyst particles from to the gas diffusion layer; only “optimal” ionomer content enables “good” ionic and electronic connections, the “good” level being of course dependent on the nature of both the ionomer and the Pt/C catalyst at stake. Despite the interest of ECSA measurements, ECSA is a static parameter, only capable to capture the utilization factor of the platinum-based catalyst; in operation, the effectiveness factor of Pt is determining [9], and it can only be assessed under real operation (current flow in H_2/air conditions), which is undertaken hereafter.

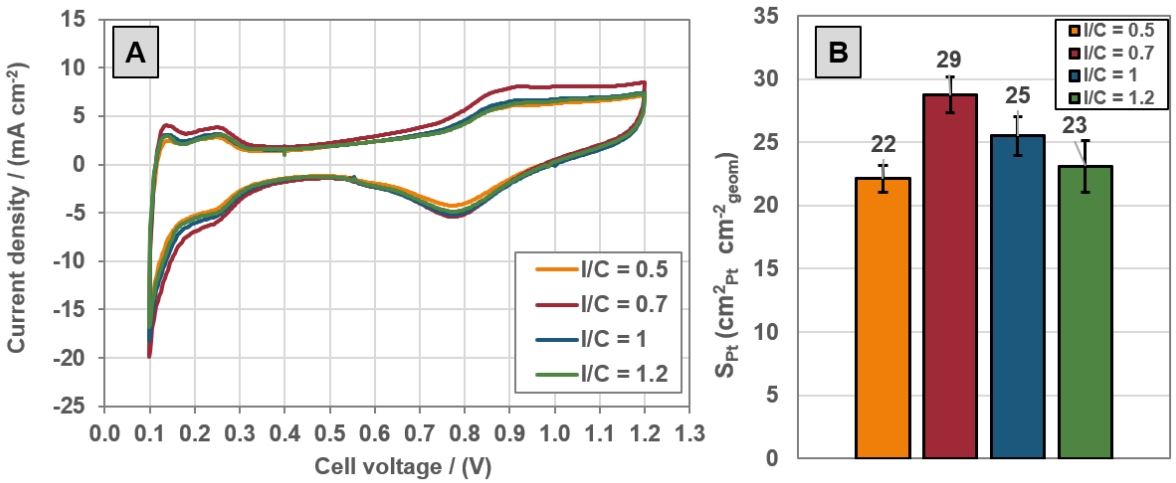

Figure 5. (A) Cyclic voltammograms obtained under H_2 / N_2, T_{cell} = 30°C, 100% RH, v = 100 mV s^{-1} for a Pt/GC cathode at various ionomer/carbon mass ratios and a Pt/VC anode; the Pt/VC anode (negative electrode in these conditions) plays the role of reference and counter-electrode, enabling to measure the base voltammogram of the Pt/GC cathode (positive electrode in these conditions); (B) Electrochemical surface area (S_{Pt}) determined from hydrogen underpotential deposition (H_{UPD} method) for the Pt/GC cathode at various ionomer/carbon ratios.

Table 2. Electrochemical surface area (ECSA, in $m^2\ g^{-1}_{Pt}$), calculated using the areal Pt loading of each Pt/GC cathode catalyst layer and the S_{Pt} values from Figure 6.

I/C ratio	ECSA ($m^2\ g^{-1}_{Pt}$)	Variation versus I/C = 0.5
0.5	24.4	-
0.7	32.2	+32%
1	27.8	+14%
1.2	25.6	+5%

The MEAs were then characterized for their performance under $H_2/(O_2 + N_2)$ (keeping P_{O2} constant at 0.4 bar for the polarization curves, **Table 1**). **Figure 6** presents the corresponding data, with Ohmic-drop corrected (IR-free) polarization curves (Figure 7A,C,E)) and high-frequency resistance measurements (Figure 7B,D,F)). **Figure 6A,B** correspond to experiments made at a temperature of T_{cell} = 80°C, an absolute back pressure of P = 2 bar abs and a relative humidity RH% = 50 at both the anode and cathode. The polarization curves in these conditions (**Figure 6A**) are plotted for MEAs using the benchmark Pt/VC anode and Pt/GC cathodes loaded at 0.1 mg_{Pt} cm^{-2} using I/C ratios of 0.5, 0.7, 1 and 1.2. **Figure 6B** gives the values of high-frequency resistance of the corresponding MEAs measured over the whole range of cell voltage (from 0.85 to 0.3 V), the cathode potential being very close to the cell voltage in these conditions: differential cells, with high-stoichiometry feed at the anode (and cathode). **Figure 6C,D** and **Figure 6E,F** provide similar sets of data for the same MEAs operated in different relative humidity values at the gas inlets: RH% = 80 and RH% = 100, respectively.

The results of **Figure 6A,C,E** (polarization curves), and **Figure SI-7** (corresponding power density curves) unambiguously demonstrate that, the I/C ratio is pivotal to MEA performance. Whatever the relative humidity tested (from 50 to 100%RH), the lowest ionomer content (I/C = 0.5) leads to significantly decreased MEA performance. The trend is more severe in dry conditions (50%RH and in a lesser extent 80%RH), in which I/C = 0.7 is still insufficient to enable proper performance. On the contrary, the highest values of I/C ratio (I/C = 1 and 1.2) lead to similar IR-free polarization curves and the highest performance recorded at any relative humidity. Taking the current density at U_{cell} = 0.6 V as a performance marker, the influence of the I/C ratio for the Pt/GC cathodes is clear (**Table 3**): an increase by more than 700% is noted at I/C = 1-1.2 versus I/C = 0.5 at 50%RH. The increase scales down to ca. 300% (a factor 4) at 80%RH and 60% at 100%RH, which can be understood easily by the fact that ionic percolation (essential to PEMFC performance) can also originate from water. These values make clear that I/C must be at least 1-1.2 to enable high PEMFC performance with a Pt/GC cathode.

Table 3. Current density (j, in A cm^{-2}) monitored at U_{cell} = 0.6 V (IR-free) versus the I/C ratio in the various conditions tested in **Figure 7**.

I/C ratio	j (A cm^{-2})			Current density variation versus I/C = 0.5		
	50%RH	80%RH	100%RH	50%RH	80%RH	100%RH
0.5	0.11	0.34	1.59	-	-	-
0.7	0.22	0.93	2.39	+100%	+173%	+50%
1	0.93	1.45	2.54	+750%	+326%	+60%
1.2	0.90	1.45	2.54	+720%	+326%	+60%

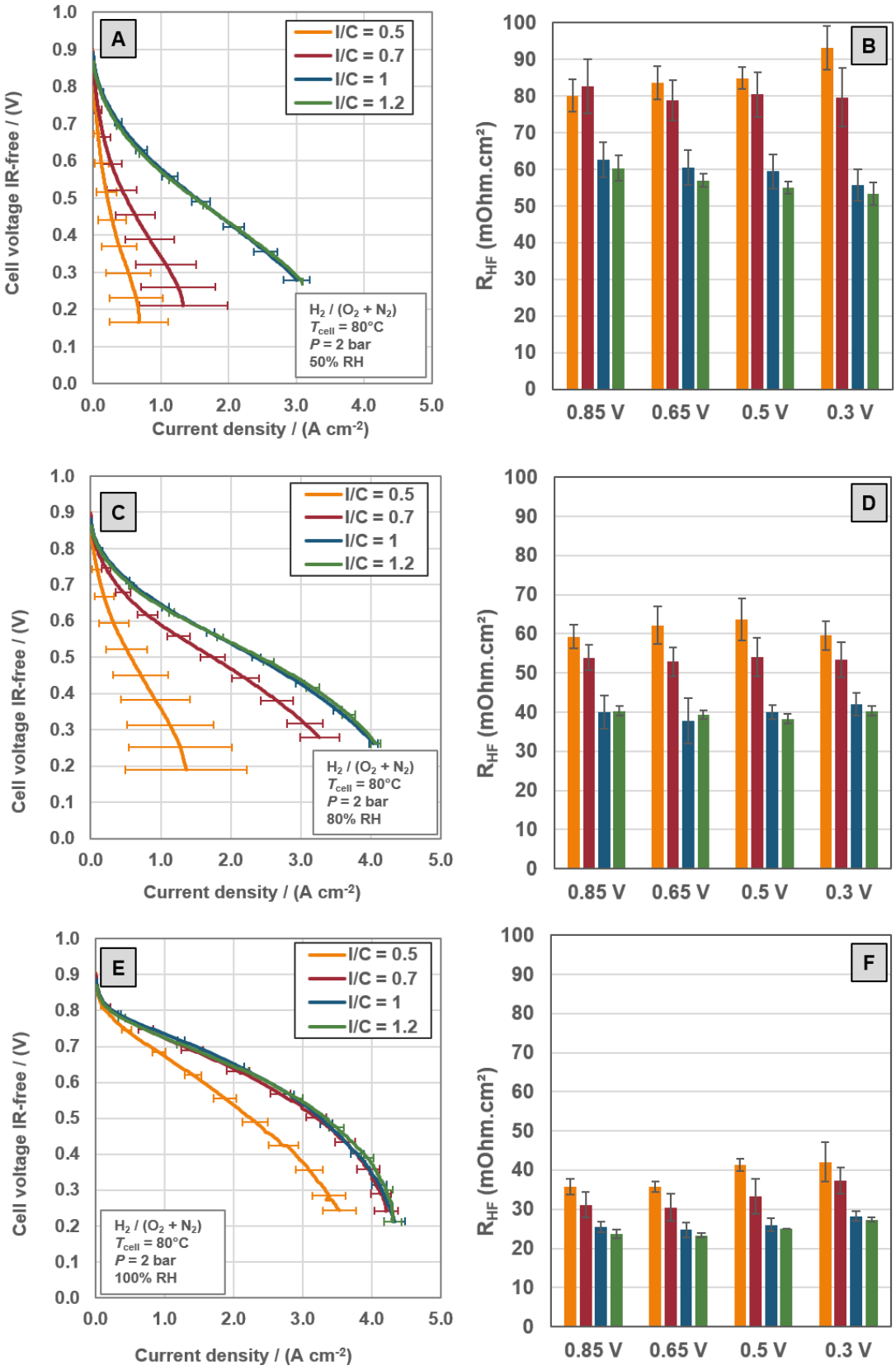

Figure 6. (A, C, E) Polarization curves and (B, D, F) high frequency resistances measured at four relevant cell voltages for MEAs prepared with Pt/GC cathode with varying I/C ratios. The tests were conducted at T_{cell} = 80°C, 2 bars absolute pressure and H_2/(O_2+N_2, 21% O_2) flows at (A, B) 50% RH, (C,

D) 80% RH and (E, F) 100% RH. The color code in the bar charts (D, E, F) corresponds to that in the polarization plots (D, E, F).

One also notes the good match between the performance and the high frequency resistances, (**Figure 6B,D,F)**, the lowest IR-free performance being recorded for MEA with the largest ohmic resistance (and the lowest I/C ratios). This could appear surprising at first sight, because the ohmic resistance is precisely corrected in the polarization curves, but this means that additional resistive terms should be considered to account for the global PEMFC performances. In other words, not only the high frequency resistance matters.

The results shown in **Figure 7** enable to shed light on this last aspect. It represents the evolution of the resistance to the proton transport in the cathode CL, measured at U_{cell} = 0.4 V under H_2/N_2 flows, according to the procedure described in section 2.7 (and in supporting information, **Figure SI-8**), adapted from [51, 52].

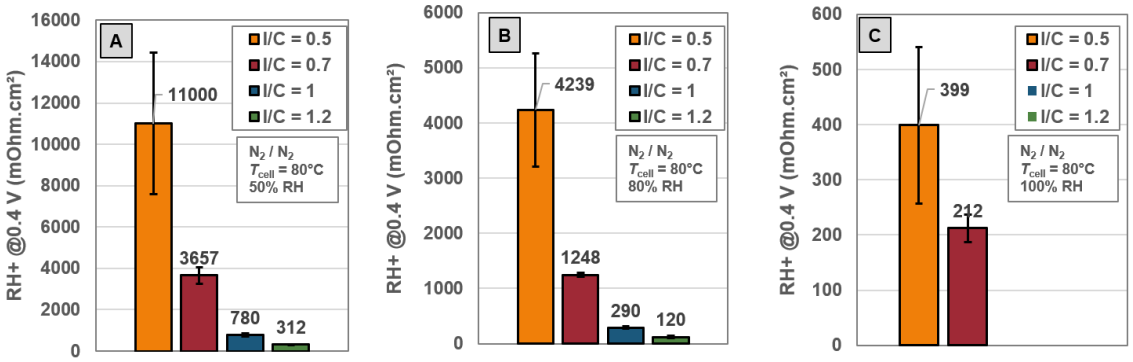

Figure 7. Proton resistance of the cathode catalyst layers for the MEAs prepared with Pt/GC cathode with varying I/C ratios. The tests were conducted at T_{cell} = 80°C and H_2/N_2 flows at (A) 50% RH, (B) 80% RH and (C) 100% RH. It must be noted that R_{H+} cannot be determined accurately for I/C = 1 or 1.2 at 100% RH (see Figure SI-9), though this value must be significantly lower than for I/C = 0.5 and 0.7.

It is very clear from **Figure 7** that the I/C ratio has an immense effect on the proton resistance (R_{H+}) in the cathode CLs, hence on the effectiveness factor of Pt [9]. The lowest I/C ratio (I/C = 0.5) results in an approximately 30-fold increase in the cathode proton resistance than the highest I/C ratio (I/C = 1.2) and this is maintained for all the relative humidity values tested. One notes though, that the proton resistance is significantly lowered when the relative humidity is large, a factor 3 of decrease in R_{H+} from 50 to 80%RH, and then another decrease in R_{H+} by a factor 5-10 from 80 to 100%RH (see **Figure SI-9**).

It is very likely that, for these materials and MEAs, the significant differences in polarization curves noted in **Figure 6A,C,E** do originate from the sharp differences of proton resistance in

their cathode CL. One also notes that the I/C ratio has a very strong effect, not only on the value of R_{H+} (which is obvious and was expected), but also on the value of the high-frequency resistance. This effect was less anticipated by the authors, and confirms the recent findings of Aït-Idir *et al.*[53]: the ionomer of the cathode CL contributes to a non-negligible extent to the high frequency resistance of the MEA, the effect being emphasized at low cathode catalyst loading (i.e. the present situation, as the cathodes are only loaded at 0.1 mg_{Pt} cm^{-2} herein).

The fact that the optimal I/C ratio is so different for Pt/GC (I/C = 1-1.2) and Pt/VC (I/C = 0.7) cathodes must be discussed. At first sight, one could think that the ink I/C ratio must be adapted to the BET area of the carbon support. Carbons with a large BET area expose a larger surface and thus need larger amount of ionomer to enable sufficient proton conduction in the CL than low BET area carbon. If one follows this hypothesis, assuming that the optimal I/C ratio for VC (S_{BET} ≈ 240 m^2 g^{-1}) is around I/C = 0.7, "optimal" inks using GC (S_{BET} ≈ 120 m^2 g^{-1}) should be ca. twice lower and that was the point in choosing a lower I/C ratio; 0.5 was tested as the lowest I/C ratio for Pt/GC, as 0.35 was presumed too small to enable any proton percolation. These new results make it very clear that the carbon BET area is not the only parameter to tune the ink composition.

One could therefore posit that the outer apparent surface area of the carbon must be the marker to choose the proper I/C ratio. The outer apparent surface area corresponds to the outer surface of the carbon particles, i.e. the carbon surface covered by the ionomer if it does not penetrate the carbon particles porosities. As both the VC and the GC supports used here roughly develop the same apparent outer surface because of the similar average carbon particle size (see **Figure 2** and associated discussion), this hypothesis would mean that the same I/C ratio must be optimal for both VC and GC based catalysts, as illustrated in the schematic representation of **Figure 8**. The optimized I/C for VC-based cathode CL in our groups is 0.7, close to "usual" values of the literature for carbon-black-based CLs (as stated in the introduction, the usual ionomer content of the dry CL is on the order of 30 wt% [12, 29]). Here, taking the same I/C value for a Pt/GC cathode CL is clearly not optimal. Although the performances are better than at I/C = 0.5, both in terms of IR-free polarization curve and values of R_{hf} and R_{H+}, they are also significantly worse than at higher I/C ratios (I/C = 1 and 1.2). This demonstrates that simple markers like the carbon BET area or apparent surface area (average diameter of the carbon particles) are not enough if one wants to predict how much ionomer to mix with the carbon-supported Pt catalyst to create inks and elaborate performant CLs.

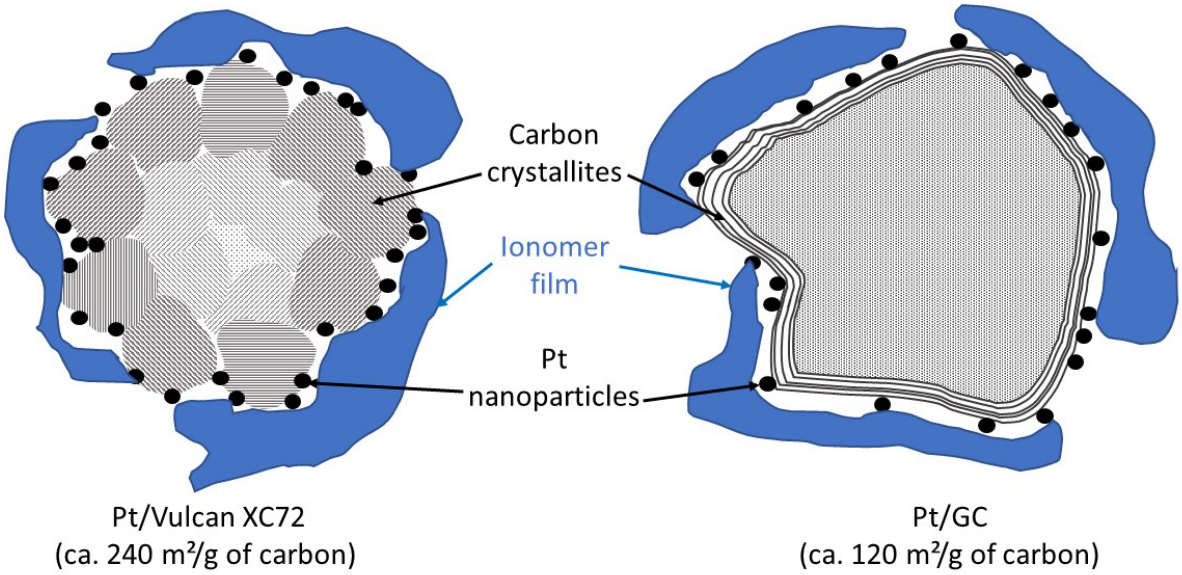

Figure 8. Schematic illustration that the ionomer content of the ink cannot simply be related to the BET area of the carbon support. Although the BET area of the Vulcan XC72 carbon support is ca. twice higher than that of the GC, the exposed (outer) area is nearly the same, so one needs (at least) as much ionomer in the ink to connect all the Pt nanoparticles when they are supported on GC (not taking into account the possible change of surface properties of the carbon, hydrophilicity, etc.).

From this, one has to conclude that the carbon surface physicochemical properties (e.g. hydrophobicity, large for graphitic carbons like GC, or hydrophilicity, large for amorphous carbons like HSAC) must also have an influence [42]. This has already been put forth by Malek *et al.* [54] a decade ago and suggests that the way the ionomer coats the carbon surface (in homogeneous thin film or possible heterogeneous pockets – those being likely at large I/C ratio, as suggested by the ECSA trend noted above) likely depends on the carbon chemistry, which are different of HSAC, Vulcan XC72 and GC. In addition, the possible presence of inner porosity, in particular mesoporosity like in mesoporous carbons or high surface area carbons, will also likely play a significant role on these surface properties: mesoporous carbons enable to better trap liquid water, in particular at low relative humidity values, and their use most likely needs to be adapted to proper I/C ratios [19, 55, 56]. In addition, the catalyst surface properties will likely also depend on the presence of Pt nanoparticles, Pt being more hydrophilic than graphitic domains of the carbon, rendering difficult any clear choice of I/C ratio [57-59]. Another parameter that makes it easier to determine the optimum I/C ratio is the ionomer volume fraction within a catalyst layer. This parameter was highlighted by Toudret et al. [47]. The final conclusion is therefore that, each time a new Pt/C catalyst will be implemented in PEMFC MEA, the proper ink recipe for its implementation in CLs will have to be evaluated, a strategy already made by trials and errors by many research laboratories. Although the optimum I/C ratio is still a difficult parameter to predict, this study presents a practical protocol for the preparation of homogeneous and high performance catalytic inks and catalyst layers using

state-of-art (Pt/VC and Pt/GC) catalysts, (Nafion) ionomer and solvents.

Of course, these conclusions might possibly not be generalized when changing the ink solvents, the type of ionomer and the type of carbon-supported Pt-based catalyst (and even less when going to non-Pt-based and/or non-carbon-based catalysts). Experimentalists and technologists of PEMFC CLs thus have a major role to play in the future, so to find a generalized methodology to tune PEMFC CLs according to the physical properties of the catalyst and ionomer components, if this is possible.

4 Conclusion

In this contribution, a thorough investigation on how to prepare Pt/VC (Vulcan XC72 carbon black-supported Pt nanoparticles) and Pt/GC (graphitized carbon black-supported Pt nanoparticles) catalyst layers of proton exchange membrane fuel cells (and notably cathode catalyst layers) is given. The experimental details concerning the ink formulation, method of mixing and deposition by blade-coating are given. The interest of the light-ball-milling method (roller mill) to mix the ink without leading to Pt/C-ionomer agglomerates and without degrading the Pt/C catalysts is demonstrated; it enables to obtain homogeneous electrodes and MEA (based on XRF spectroscopy and SEM on surface and cross-section analyses).

These methods, allow to show that for Pt/GC CLs, the proper ionomer-to-carbon ratio cannot be chosen identical to the optimal one for Pt/VC CLs. For Pt/GC cathodes, the optimal I/C ratio must be high (1-1.2), and this clearly improves the current density at 0.6 V compared to cathodes CLs with I/C = 0.5 (+700%, +300 and +60% at 50%, 80% and 100% RH, respectively). Of course, the effect of the I/C ratio is not as dramatic when the RH% is high (e.g. 100%RH), even if better PEMFC performance are always monitored (regardless the %RH value) at the optimal I/C ratio.

The proper I/C ratio does neither directly depend on the BET surface area of the carbon substrate, nor on its outer apparent surface (average apparent carbon particles diameter). It rather seems that the physicochemical surface properties of the Pt/GC sample must also be considered, which means that a proper tuning of the I/C ratio must be made each time a Pt/C catalyst is investigated.

5 Acknowledgements

CL, MH, JFB and MC thank the Carnot Energies du Futur (Carnot-EF, OPTIPEM project), and the “France 2030” government investment plan managed by the French National Research Agency (PEMFC95 project, grant ANR-22-PEHY-0005) for funding the post-doctorate of CL. Some of this work has been performed within the framework of the Centre of Excellence of Multifunctional Architectured Materials “CEMAM”, Grenoble France n◦ ANR-10-LABX-44–01.

6 Authors contributions

CL made the experiments and drafted the results. MC, MH and JFB conceived the study. All the authors participated to the drafting and the corrections of the paper.

7 References

[1] A.F. Ghoniem, Needs, resources and climate change: Clean and efficient conversion technologies, Prog. Energ. Comb. Sci., 37 (2011) 15-51.
[2] T.M. Gür, Review of electrical energy storage technologies, materials and systems: challenges and prospects for large-scale grid storage, Energy Environ. Sci., 11 (2018) 2696-2767.
[3] M. Götz, J. Lefebvre, F. Mörs, A. McDaniel Koch, F. Graf, S. Bajohr, R. Reimert, T. Kolb, Renewable Power-to-Gas: A technological and economic review, Renew. Energy, 85 (2016) 1371-1390.
[4] X.X. Wang, M.T. Swihart, G. Wu, Achievements, challenges and perspectives on cathode catalysts in proton exchange membrane fuel cells for transportation, Nature Catalysis, 2 (2019) 578-589.
[5] L. Dubau, L. Castanheira, M. Chatenet, F. Maillard, J. Dillet, G. Maranzana, S. Abbou, O. Lottin, G. De Moor, A. El Kaddouri, C. Bas, L. Flandin, E. Rossinot, N. Caqué, Carbon corrosion induced by membrane failure: The weak link of PEMFC long-term performance, Int. J. Hydrogen Energy, 39 (2014) 21902-21914.
[6] L. Dubau, L. Castanheira, F. Maillard, M. Chatenet, O. Lottin, G. Maranzana, J. Dillet, A. Lamibrac, J.-C. Perrin, E. Moukheiber, A. ElKaddouri, G. De Moor, C. Bas, L. Flandin, N. Caqué, A review of PEM fuel cell durability: materials degradation, local heterogeneities of aging and possible mitigation strategies, WIRES Energy Environ., 3 (2014) 540-560.
[7] A. Ly, T. Asset, P. Atanassov, Integrating nanostructured Pt-based electrocatalysts in proton exchange membrane fuel cells, J. Power Sources, 478 (2020) 228516.
[8] S. Hidekazu, T. Takeshi, N. Yuri, I. Yoshiko, M. Atsuo, K. Yuichi, K. Maito, M. Hidetoshi, U. Suguru, K. Yuki, Nanostructural Evolution during Catalyst Layer Formation Studied via Cryo-Electron Microscopy, ECS Trans., 80 (2017) 253-258.
[9] M. Chatenet, L. Dubau, N. Job, F. Maillard, The (electro)catalyst | membrane interface in the Proton Exchange Membrane Fuel Cell: similarities and differences with non-electrochemical Catalytic Membrane Reactors, Catal. Today, 156 (2010) 76-86.
[10] S. Woo, S. Lee, A.Z. Taning, T.H. Yang, S.H. Park, S.D. Yim, Current understanding of catalyst/ionomer interfacial structure and phenomena affecting the oxygen reduction reaction in cathode catalyst layers of proton exchange membrane fuel cells, Current Opinion in Electrochemistry, 21 (2020) 289-296.

[11] H. Steven, Fuel Cell Catalyst Layers: A Polymer Science Perspective, Chem. Mater., 26 (2013) 381-393.
[12] S. Litster, G. McLean, PEM fuel cell electrodes, J. Power Sources, 130 (2004) 61-76.
[13] E. Passalacqua, F. Lufrano, G. Squadrito, A. Patti, L. Giorgi, Nafion content in the catalyst layer of polymer electrolyte fuel cells: effects on structure and performance, Electrochim. Acta, 46 (2001) 799-805.
[14] G. Bender, T.A. Zawodzinski, A.P. Saab, Fabrication of high precision PEFC membrane electrode assemblies, J. Power Sources, 124 (2003) 114-117.
[15] S.S. Kocha, Principle of MEA preparation, in: W. Vielstich, A. Lamm, H.A. Gasteiger (Eds.) Handbook of Fuel Cells, Wiley, Chichester, 2003, pp. 538-565.
[16] M.B. Sassin, Y. Garsany, B.D. Gould, K.E. Swider-Lyons, Fabrication Method for Laboratory-Scale High-Performance Membrane Electrode Assemblies for Fuel Cells, Anal. Chem., 89 (2017) 511-518.
[17] Z. Turtayeva, F. Xu, J. Dillet, K. Mozet, R. Peignier, A. Celzard, G. Maranzana, Manufacturing catalyst-coated membranes by ultrasonic spray deposition for PEMFC: Identification of key parameters and their impact on PEMFC performance, Int. J. Hydrogen Energy, 47 (2022) 16165-16178.
[18] A. Orfanidi, P. Madkikar, H.A. El-Sayed, G.S. Harzer, T. Kratky, H.A. Gasteiger, The Key to High Performance Low Pt Loaded Electrodes, J. Electrochem. Soc., 164 (2017) F418.
[19] Y. Zeng, J. Liang, B. Li, H. Yu, B. Zhang, K.S. Reeves, D.A. Cullen, X. Li, D. Su, G. Wang, S. Zhong, H. Xu, N. Macauley, G. Wu, Pt Nanoparticles on Atomic-Metal-Rich Carbon for Heavy-Duty Fuel Cell Catalysts: Durability Enhancement and Degradation Behavior in Membrane Electrode Assemblies, ACS Catal., 13 (2023) 11871-11882.
[20] M. Chen, C. Zhao, F. Sun, J. Fan, H. Li, H. Wang, Research progress of catalyst layer and interlayer interface structures in membrane electrode assembly (MEA) for proton exchange membrane fuel cell (PEMFC) system, eTransportation, 5 (2020) 100075.
[21] S.A. Berlinger, B.D. McCloskey, A.Z. Weber, Inherent Acidity of Perfluorosulfonic Acid Ionomer Dispersions and Implications for Ink Aggregation, J. Phys. Chem. B, 122 (2018) 7790-7796.
[22] S.A. Berlinger, B.D. McCloskey, A.Z. Weber, Probing Ionomer Interactions with Electrocatalyst Particles in Solution, ACS Energy Letters, 6 (2021) 2275-2282.
[23] S.A. Berlinger, S. Garg, A.Z. Weber, Multicomponent, multiphase interactions in fuel-cell inks, Current Opinion in Electrochemistry, 29 (2021) 100744.
[24] S.A. Berlinger, A. Chowdhury, T. Van Cleve, A. He, N. Dagan, K.C. Neyerlin, B.D. McCloskey, C.J. Radke, A.Z. Weber, Impact of Platinum Primary Particle Loading on Fuel Cell Performance: Insights from Catalyst/Ionomer Ink Interactions, ACS Applied Materials & Interfaces, 14 (2022) 36731-36740.
[25] M. Wang, J.H. Park, S. Kabir, K.C. Neyerlin, N.N. Kariuki, H. Lv, V.R. Stamenkovic, D.J. Myers, M. Ulsh, S.A. Mauger, Impact of Catalyst Ink Dispersing Methodology on Fuel Cell Performance Using in-Situ X-ray Scattering, ACS Applied Energy Materials, 2 (2019) 6417-6427.
[26] T.A.M. Suter, K. Smith, J. Hack, L. Rasha, Z. Rana, G.M.A. Angel, P.R. Shearing, T.S. Miller, D.J.L. Brett, Engineering Catalyst Layers for Next-Generation Polymer Electrolyte Fuel Cells: A Review of Design, Materials, and Methods, Advanced Energy Materials, 11 (2021) 2101025.
[27] S. Shahgaldi, I. Alaefour, X. Li, Impact of manufacturing processes on proton exchange membrane fuel cell performance, Applied Energy, 225 (2018) 1022-1032.
[28] M. Bahrami, Y. Chen, N. Kumar, F.P. Orfino, M. Dutta, M. Lauritzen, E. Setzler, A.L. Agapov, E. Kjeang, Improved Decal Transfer Method to Reduce Membrane Damage from Foreign Particles in Membrane Electrode Assembly, J. Electrochem. Soc., 170 (2023) 114527.
[29] S. Woo, S. Lee, A.Z. Taning, T.-H. Yang, S.-H. Park, S.-D. Yim, Current understanding of catalyst/ionomer interfacial structure and phenomena affecting the oxygen reduction reaction in cathode catalyst layers of proton exchange membrane fuel cells, Current Opinion in Electrochemistry, 21 (2020) 289-296.

[30] S. Holdcroft, Fuel Cell Catalyst Layers: A Polymer Science Perspective, Chem. Mater., 26 (2014) 381-393.
[31] A. Orfanidi, P.J. Rheinländer, N. Schulte, H.A. Gasteiger, Ink Solvent Dependence of the Ionomer Distribution in the Catalyst Layer of a PEMFC, J. Electrochem. Soc., 165 (2018) F1254-F1263.
[32] C.M. Baez-Cotto, J.P. Pfeilsticker, A.O. Godoy, M. Batool, S. Zaccarine, M. Wang, O. Bird, S. Pylypenko, J. Jankovic, M. Ulsh, S. Mauger, The effect of ink ball milling time on interparticle interactions and ink microstructure and their influence on crack formation in rod-coated catalyst layers, J. Power Sources, 583 (2023) 233567.
[33] C.H. Song, J.-S. Park, Effect of Dispersion Solvents in Catalyst Inks on the Performance and Durability of Catalyst Layers in Proton Exchange Membrane Fuel Cells, Energies, 12 (2019) 549.
[34] C. Lei, F. Yang, N. Macauley, M. Spinetta, G. Purdy, J. Jankovic, D.A. Cullen, K.L. More, Y.S. Kim, H. Xu, Impact of Catalyst Ink Dispersing Solvent on PEM Fuel Cell Performance and Durability, J. Electrochem. Soc., 168 (2021) 044517.
[35] L. Castanheira, L. Dubau, M. Mermoux, G. Berthomé, N. Caqué, E. Rossinot, M. Chatenet, F. Maillard, Carbon Corrosion in Proton-Exchange Membrane Fuel Cells: From Model Experiments to Real-Life Operation in Membrane Electrode Assemblies, ACS Catal., 4 (2014) 2258-2267.
[36] L. Castanheira, W.O. Silva, F.H.B. Lima, A. Crisci, L. Dubau, F. Maillard, Carbon corrosion in proton-exchange membrane fuel cells: Effect of the carbon structure, the degradation protocol, and the gas atmosphere, ACS Catal., 5 (2015) 2184-2194.
[37] M. Bernt, A. Siebel, H.A. Gasteiger, Analysis of voltage losses in PEM water electrolyzers with low platinum group metal loadings, J. Electrochem. Soc., 165 (2018) F305-F314.
[38] G.S. Harzer, J.N. Schwämmlein, A.M. Damjanović, S. Ghosh, H.A. Gasteiger, Cathode Loading Impact on Voltage Cycling Induced PEMFC Degradation: A Voltage Loss Analysis, J. Electrochem. Soc., 165 (2018) F3118-F3131.
[39] M. Lopez-Haro, L. Guétaz, T. Printemps, A. Morin, S. Escribano, P.H. Jouneau, P. Bayle-Guillemaud, F. Chandezon, G. Gebel, Three-dimensional analysis of Nafion layers in fuel cell electrodes, Nature Communications, 5 (2015).
[40] R. Riasse, C. Lafforgue, F. Vandenberghe, F. Micoud, A. Morin, M. Arenz, J. Durst, M. Chatenet, Benchmarking proton exchange membrane fuel cell cathode catalyst at high current density: A comparison between the rotating disk electrode, the gas diffusion electrode and differential cell, J. Power Sources, 556 (2023) 232491.
[41] T. Lazaridis, H.A. Gasteiger, Pt-catalyzed oxidation of PEMFC carbon supports: A path to highly accessible carbon morphologies and implications for start-up/shut-down degradation, J. Electrochem. Soc., 168 (2021).
[42] F. Chabot, L. Porcar, L. Guetaz, S. Rosini, A. Morin, Tracking the evolution of ionomer film and catalyst material to unravel PEMFC performance degradation, In preparation, (2024).
[43] A.B. Sarah, D.M. Bryan, Z.W. Adam, Understanding Binary Interactions in Fuel-Cell Catalyst-Layer Inks, ECS Meeting Abstracts, MA2017-02 (2017) 1390-1390.
[44] S.A. Berlinger, A. Chowdhury, T. Van Cleve, A. He, N. Dagan, K.C. Neyerlin, B.D. McCloskey, C.J. Radke, A.Z. Weber, Impact of Platinum Primary Particle Loading on Fuel Cell Performance: Insights from Catalyst/Ionomer Ink Interactions, ACS Applied Materials and Interfaces, 14 (2022) 36731-36740.
[45] R. Sgarbi, W. Ait Idir, Q. Labarde, M. Mermoux, P. Wu, J. Mainka, J. Dillet, C. Marty, F. Micoud, O. Lottin, M. Chatenet, Does the platinum-loading in proton-exchange membrane fuel cell cathodes influence the durability of the membrane-electrode assembly?, Industrial Chemistry & Materials, 1 (2023) 501-515.
[46] H. Xu, E.L. Brosha, F.H. Garzon, F. Uribe, M. Wilson, B. Pivovar, The Effect of Electrode Ink Processing and Composition on Catalyst Utilization, ECS Trans., 11 (2007) 383-391.
[47] P. Toudret, A. Chennevière, J.-F. Blachot, G. Gébel, M. Heitzmann, A. Morin, Evidence of well-dispersed ionomer in the cathode catalyst layer of proton exchange membrane fuel cell by small angle scattering, and effect of its content on performance, In preparation, (2024).

[48] I. Gatto, A. Saccà, D. Sebastián, V. Baglio, A.S. Aricò, C. Oldani, L. Merlo, A. Carbone, Influence of Ionomer Content in the Catalytic Layer of MEAs Based on Aquivion® Ionomer, in: Polymers, 2021, pp. 3832.
[49] T. Suzuki, S. Tsushima, S. Hirai, Effects of Nafion® ionomer and carbon particles on structure formation in a proton-exchange membrane fuel cell catalyst layer fabricated by the decal-transfer method, Int. J. Hydrogen Energy, 36 (2011) 12361-12369.
[50] M.R. Lee, H.Y. Lee, S.D. Yim, C.S. Kim, Y.G. Shul, A. Kucernak, D. Shin, Effects of Ionomer Carbon Ratio and Ionomer Dispersity on the Performance and Durability of MEAs, Fuel Cells, 18 (2018) 129-136.
[51] T. Gaumont, Protonic resistance of proton exchange membrane fuel cells (PEMFC) : effects of humidity and degradations, in: PhD Thesis, LEMTA, Université de Lorraine, Nancy, France, 2017.
[52] F. Vandenberghe, Towards a better understanding and modeling of catalyst and catalyst layer operation in Proton Exchange Membrane Fuel Cell, in: PhD Thesis, CEA-LITEN, University Grenoble Alpe, Grenoble, France, 2022.
[53] W. Aït-Idir, P. Wu, R. Sgarbi, Q. Labarde, S. Touhami, M. Daoudi, A. El kaddouri, J.-C. Perrin, J. Dillet, C. Marty, F. Micoud, M. Chatenet, O. Lottin, J. Mainka, Oxygen diffusion impedance in proton exchange membrane fuel cells – insights into electrochemical impedance spectra and equivalent electrical circuit modeling, Electrochim. Acta, 472 (2023) 143430.
[54] K. Malek, T. Mashio, M. Eikerling, Microstructure of Catalyst Layers in PEM Fuel Cells Redefined: A Computational Approach, Electrocatal., 2 (2011) 141.
[55] K. Kodama, T. Suzuki, K. Shinozaki, R. Jinnouchi, Translating insights from experimental analyses with single-crystal electrodes to practically-applicable material development strategies for controlling the Pt/ionomer interface in polymer electrolyte fuel cells, Journal of Physics: Energy, 5 (2023) 014018.
[56] S. Gottesfeld, Editors' Choice—Review—Polymer Electrolyte Fuel Cell Science and Technology: Highlighting a General Mechanistic Pattern and a General Rate Expression for Electrocatalytic Processes, J. Electrochem. Soc., 169 (2022).
[57] Q.P. Wang, M. Eikerling, D.T. Song, Z.S. Liu, Modeling of ultrathin two-phase catalyst layers in PEFCs, J. Electrochem. Soc., 154 (2007) F95-F101.
[58] J. Liu, M. Eikerling, Model of cathode catalyst layers for polymer electrolyte fuel cells: The role of porous structure and water accumulation, Electrochim. Acta, 53 (2008) 4435-4446.
[59] Z. Xia, Q. Wang, M. Eikerling, Z. Liu, Effectiveness factor of Pt utilization in cathode catalyst layer of polymer electrolyte fuel cells, Can. J. Chem., 86 (2008) 657-667.